# Drillstring Failure - Identification, Modelling and Experimental Characterization

**Jamil Abdo**
Department of Mechanical and Aerospace Engineering
Utah State University
Logan, UT, USA

**Khaled Boulbrachene**
Department of Chemistry and Earth Sciences
Qatar University
Doha, Qatar

**Edris m. Hassn**
Department of Chemistry and Earth Sciences
Qatar University
Doha, Qatar

**Jan C.T. Kwak**
Department of Chemistry and Earth Sciences
Qatar University
Doha, Qatar

**Keywords:** Drill String Failure, Drill string Safety, Fatigue Failure, Lateral and Torsional Vibration.

## ABSTRACT

Drilling is one of the most costly and risky activities in oil and gas industry due to complexity of interactions with downhole formation. Under such conditions, the uncertainty of drillstring behavior increase and hence it becomes difficult to predict the causes, occurrences, and types of failures. Lateral and torsional vibrations often cause failure of Bottom Hole Assembly (BHA), drillstring failure, drill bit and wall borehole damages. In this work, a model is presented to determine the impact of lateral and torsional vibrations on a drillstring during the drilling operation. The model aims to mimic real drillstring behavior inside a wellbore with regards to its dynamic movements due to multiple real situations such as eccentricity of collars, drill pipe sections, and stick-slip phenomena occurring due to the interaction of the bit and the drill string with the well formation. The work aims to develop a basis for determining critical operating speeds and design parameters to provide safe drilling procedures and reduce drill string fatigue failure. Lagrangian approach is used in this study to attain drill string lateral and torsional vibration coupling equations. The nonlinear equations are solved numerically to obtain the response of the system. In this work, we also present a brief description of an in-house constructed experimental setup. The setup has the capability to imitate the downhole lateral and torsional vibration modes. Parameters from the experimental investigations are incorporated for validation of the mathematical models and for prediction of the drill string fatigue life. Such investigations are essential for oil/gas industries as they provide solutions as well as recommendations about operating speed, lateral and torsional amplitudes measurements and corrections, and the conditions for avoiding occurrence of natural frequency(ies) of the system.

## INTRODUCTION

Despite huge advances in technology and unconventional fossil fuel recovery, drilling a well is still the primary technique for extracting oil and natural gas. This process is highly complicated with huge systems being utilized for drilling.

In drilling of oil and gas wells, severe shock and vibrations occur that are detrimental to the service life of drillstrings and down-hole assembly tools. The causes of these vibrations are due to complex surroundings and a lot of uncertainties include impact and friction at the interfaces of borehole/drillstring and bit/ hard-rock formation, imbalances, drillstring eccentricity or initial curvature in the drill collar sections, various linear or non-linear resonances [1-3].

There are three modes of vibration mainly axial, lateral, and torsional, which indicate direction and response of the drillstring when it runs into trouble downhole [4]. In axial mode, the vibration is longitudinal motion along the drillstring resulting in tension and occasionally compression-tension reversals when the bit comes across hard formation while cutting through loose formation at high speed (also known as bit-bounce). In lateral mode, the vibration is side to side motion that causes flexing or bending of components again leading to stress reversals where one side is in a different tensional state from the other. In torsional mode, the vibration is resistance to the rotation resulting in twisting as torque is applied to overcome resistance. As a result of such torsional vibrations, the angular velocity of rotary surface may vary with time. Bit formation interaction, drillstring–wellbore contacts, mass imbalance, lateral shocks, bit, BHA whirl and stick-slip are the main sources of these vibration modes.

Drillstring fatigue failure is very common due to generation of single and coupled vibration modes and mechanisms. These severe vibrations often cause failures of BHA tool, drill pipe abrasive wear, drill bit and wall borehole damages, reduction of the rate of penetration (ROP), and consequently incur high costs [5-6].

Several attempts have been made to study the drillstring vibrations and to overcome the difficulties encountered by field engineers. Laboratory testing to investigate lateral behavior of a

part of a drill string represented by a rod and subjected to axial loading was highlighted in [7]. The experimental set-up takes into account the curvature of the rod, mud, stabilizers and rotational speed. The lateral behavior of the drill string subjected to axial excitations of the drill bit is governed by time varying parameter equations due to torsion-lateral and longitudinal-lateral couplings. The dynamic stability of drill strings has been studied by Yigit and Christofourou [8]. In their study transverse vibrations induced by axial loading in a drill string modeled by a uniform slender beam undergoing axial and transverse deformations. Non rotating drill strings are considered and all deformations are assumed to occur in a single plane. The transverse motion of the beam is conned by the borehole and is assumed to be adequately modeled by Euler-Bernoulli beam theory. In the problem formulation, linear and nonlinear coupling were retained which leads to fully coupled differential equations. A method was suggested in [9] to examine some of the drilling technology factors that can affect drill string fatigue behavior. Such drilling technology factors include tensile load, torque, abrasive wear and mud corrosion. Alternative approximate techniques to determine the amplitudes of the limit cycles that evolve from stick-slip vibrations were carried out in [10]. Approximate closed-form equations were derived for normal and tangential contact forces of rough surfaces in dry friction in [11]. Some other approaches were suggested for the analysis of some of the drilling technology factors that can affect the drilling string fatigue behavior. Comparative study of full-scale fatigue test results and field data were accordingly presented in [12-14]. Such drilling factors include threaded connections. A full scale mathematical modeling to predict fatigue life in a threaded connection is proposed in [15].

Modeling of coupled axial, lateral, and torsional vibrations of drill strings has been presented in [16]. In this model, governing equations of motion for a drill string considering coupling between axial, lateral and torsional vibrations were obtained using Lagrangian approach. Many studies on drill string dynamics are mostly concerned with axial and tensional vibrations. Coupling between these two motions has been discussed in [17] where some measuring tools were developed to estimate axial force, torque, axial and rotational motions at the top of a drill string. Equations of motion for coupled torsional and bending vibrations were obtained in [18] through a simplified model with equivalent lumped parameters. The dynamic response of a drill string was obtained by a numerical solution of equations. Case studies based on downhole measurements were presented in [19]. Several important types of vibration, including forward and backward whirl, linear coupling between WOB and lateral vibration, and bit bounce were illustrated. The case studies have also considered bending vibration of rotating and nonrotating drill string as well as whirling and parametric instabilities. Dynamic behavior of a section of whirling drill collars were analyzed in terms of rotor dynamics, with account taken of the non-linear influences caused by drilling fluid, stabilizer clearance and stabilizer friction [20]. An effective means of minimizing torsional vibrations, and thus improving coring performance, using an active-damping system was developed for electrical rotary drives in deep seas exploration operations [21]. The research work in [22-28] has investigated stability of drill string considering three simple mechanical systems representing string-torsional vibration, bit-lateral dynamics, and coupled torsional-lateral vibration of the bit string assembly.

It is well-known that the drillstring and downhole tool failure usually occurs from failing to control one or more of the vibration mechanisms. However, so far all models were not able to accurately determine drillstring design parameters. The current work is motivated by the fact that the solutions should start with the ability to measure different modes and hence identify the different vibration mechanisms. In contrary to previous research, this work aims to imitate real drillstring behavior inside the wellbore with regards to its dynamic movements based on modeling an in-house constructed testing rig which mimic the real drilling field operations. In addition, this work develops a basis for determining the critical operating speeds and design parameters to provide a basis for developing safe drilling procedures and developing fatigue failure models that can predict the safe operating life of equipment under such loads. This procedure should pave the way for future work involve developing an accurate drillstring buckling, stick-slip, and lock-up failure models.

In general, in modeling axial vibration approaches are mainly based on modeling an undamped oscillation of a bar and developing its governing linear partial differential equation considering different scenarios through a variety of boundary conditions and damping effects. For lateral vibration, beam theory is commonly utilized to study the flexural modes of the drillstring while employing dynamic lumped models to study the lateral displacement and the behavior of the drillstring. Torsional vibrations are mainly modeled using modified versions of the torsional pendulum. Coupled versions of these models are also exist in order to capture more complex behavior with higher fidelity such as the axial-torsional and torsional-bending models. However, none of these models were able to accurately predict the drillstring behavior and its failure modes or to provide an accurate estimates about the drillstring critical speed, deflection or critical frequency.

The current work offers a mechanical performance description of a complex nonlinear dynamics of drillstrings as well as provides a lumped parameters model which can be readily used for other slender rotatory components subjected to fatigue loading. The testing rig induces these vibration modes as well as facilitates measurements of lateral and torsional vibrations.

Limitations of the proposed experimental drillstring induced vibration testing rig include scaling issues (domain size effect)

and some difficulties in simulating the real downhole vibrations. Field experiments, on the other hand, are not broadly used for cross-validation of the performance of drillstrings under such vibration modes. One more testing procedure that was not conducted in this work is modify the testing facility so it can be readily accommodate testing of the threaded connections of the tool joints. The mechanism of fatigue failure in the tool joint of the drillstring plays a role in drillstring serviceability.

This paper aims at gaining deeper understanding of the complex behavior of drillstring under vibrations and its detrimental effect on drilling operation. The Lagrangian approach is used to obtain the drill pipe lateral and torsional vibration coupling equations of motion. The mathematical model is expressed in terms of four independent degrees of freedom. The effects of bending and torsion vibrations, and whirling motion of the drillstring are included in the model. The nonlinear equations are solved numerically to obtain the response. The experimental setup provides further development of a more comprehensive testing of drillstring. It can readily accommodate other relevant effects such as wellbore and drill string contact, drill string and mudflow interaction and stick-slip phenomena. Fatigue life is also measured from the number of cycles associated with the amplitude of the stress cycles created due to lateral vibration Results showed that drill string size and lateral vibration stress cycles have significant effects on the fatigue life of the drillstring.

## MATHEETICAL MODELING

In this work a mathematical model that accounts for the effects of lateral and torsional vibrations on a drillstring generated due to the interaction of the drillstring with the formation during the drilling operation is formulated. Modeling of such rotating component is highly non-linear and complex due to contact behavior and dynamics of the drillstring which involve broad vibration profiles include axial, lateral and torsional modes. The force applied on the bit, termed Weight-on-Bit (WOB) is the essential force in drilling process. WOB affects rate of penetration as well as natural frequencies. The lower portion of the drill collars is assumed to be under combined torsional and lateral vibrations. Lateral vibrations are recognized as the leading cause of drillstring and bottom hole assembly (BHA) failures, and the most destructive type of vibration in creating large shocks as the BHA impacts with the wellbore. Drillstrings are considered to be a slender systems, and it is known that for highly slender rotating structures (i.e., systems with large length to diameter ratios), lateral and torsional vibrations are strongly coupled. In such situation the effect of axial vibration due to bit bounce caused by axial loading on the drillstring failure is less compare to other types of vibration. However, the effect of coupled three modes of vibration (Lateral, Torsional and Axial) on drillstring failure is intended to be a future work. Introducing axial vibration would require major modifications in the experimental setup.

In such a problem, it is convenient to model it as a simple Jeffcott rotor model. The Jeffcot rotor model is capable of retaining crucial characteristics of a rotor in its imbalance response. A schematic diagram of the unbalanced mass and rotor system is shown in Fig. 1.

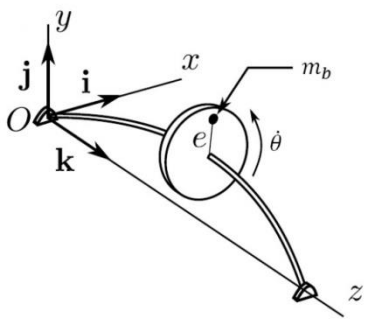


**Fig. 1.** Representation diagram for the equivalent model

The model consists of two rigid frictionless bearings, an elastic isotropic shaft, and a rigid disk located at the center of the shaft. The proposed model imitates the built-in experimental setup and captures its dynamic response for different system's parameters.

Jeffcott lumped-parameter model have been used to adequately describe the dynamics response of a rotary drillstring. The model was used to study the nonlinear dynamics of the drillstring and its kinematic behavior. Jeffcott model has been conveniently considered to investigate the drillstring fatigue failure where amplitudes of lateral vibrations due to eccentricity of mass and angle of twist as a result of applied torques were captured precisely. It is known that fatigue failure happens when a structure is subjected to cyclic (fluctuated) stresses which is associated with lateral amplitudes and twisting angle, hence Jeffcott rotor model was found advantageous for this study. Jeffcott rotor model has yielded a motion of the rotor that was much more comparable to the experimental work [29-34].

In the proposed model, an unbalance mass $m_b$ is attached to the rotor of mass $M$ and mass moment of inertia $I_o$ at distance $e$ represent eccentricity with respect to its geometrical center. The lumped parameter model is shown in Fig. 2. The rotor is assumed to be symmetrical such that the lateral stiffnesses and lateral damping have an equivalent spring constants and damping coefficients of $k_x = k_y = k_b$ and $c_x = c_y = c_b$, respectively. Torsional motion is represented by dissipating and conservative components defined by the damping coefficient $c_{tor}$ and the spring constant $k_{tor}$. The degrees of freedom can be described by three orthogonal unit vectors, namely, $(a_1\ ,a_2)$, $(b_1,\ b_2)$ and $(c_1,\ c_2)$. The unit vectors are projected into $x$ and $y$ coordinates and fixed at the origin $O$. Both $(b_1, b_2)$ $(c_1, c_2)$ unit vectors are fixed at the geometrical center of the rotor and allowed to rotate. The reference frame $(b_1, b_2)$ is allowed to rotate at a constant angular speed $(\dot{\theta})$ with respect to $(a_1\ ,a_2)$ reference frame. Therefore, the angle between $a_1$ and $b_1$ defines rigid body

rotation $\theta$. The torsional deformation ($\gamma$) is defined as the angle between $b_1$ and $c_1$.

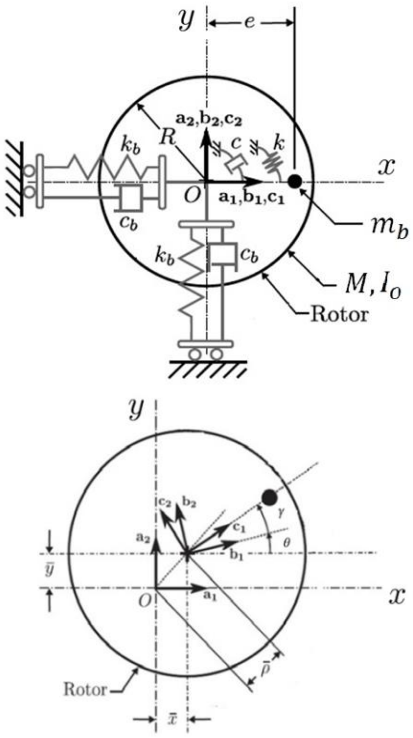


**Fig. 2.** Lumped parameter model

In this setting, when the rotor is at rest, all unit vectors coincide. Once a drive speed ($\dot{\theta}$) is introduced, the rotor moves away from the origin *O* due to the effect of the centrifugal force acting on it. As a result, the rotor's geometrical center is displaced to the point $(\tilde{x}, \tilde{y})$. In addition, it is assumed that the rotor is only able to undergo planar motions with no gyroscopic effects due to rotations about the x and y axes. A constraint is imposed as $a_3 = b_3 = c_3$ at the entire time *t*, where $a_3 = a_1$ x $a_2$, $b_3 = b_1$ x $b_2$ and $c_3 = c_1$ x $c_2$. In order to retain generality, eccentricity is (*e*) initially parallel to the x-axis.

In Fig. 2, the angle $\beta$ is defined as follows:

$$\beta = \theta + \gamma \tag{1}$$

Thus, $\beta$ represents the total angular displacement of the rotor. Taking time derivative of Eq. (1) results in:

$$\dot{\beta} = \dot{\theta} + \dot{\gamma} \tag{2}$$

where $\dot{\beta}$ represent the total angular speed of the rotor. By normalizing $\dot{\beta}$ with respect to $\dot{\theta}$ we get:

$$\dot{\beta}_{norm} = \frac{\dot{\beta}}{\dot{\theta}} \tag{3}$$

**EQUATIONS OF MOTION:**

There are mainly three approaches that could be used to derivate the governing equations of a dynamic system, namely, Hamilton's principle, Lagrange principle or direct equilibrium using d' Alembert's principle. Both Hamilton and Lagrange are energy principles which derive the equations of motion by considering the system from an overall perspective, without the need to identify the internal forces at the interconnections of the system's components as it is the case in the vector based d' Alembert's principle. Therefore, in modeling drillstring it is simpler to consider energy principal as energy is a scalar quantity, independent on the choice of coordinate system and can easily deal with multi-degrees of freedom systems with the help of the generalized coordinates which describe the system. In addition, while Hamilton's principle uses an integral based approach, Lagrange principle is a differential approach which requires considerably less computational effort. Therefore, in this work, Lagrange's equation is used to derive the system's equations of motion.

$$L = T - U \tag{4}$$

$$\frac{d}{dt}\left(\frac{\delta L}{\delta \dot{q}_i}\right) - \frac{\delta L}{\delta q_i} + \frac{\delta D}{\delta \dot{q}_i} = F_i \tag{5}$$

where:
$q_i$: generalized coordinate (Degree of Freedom).
$D$: Rayleigh dissipation function.
$F_i$: generalized force along a particular generalized coordinate.

**KINETIC AND POTENTIAL ENERGIES**

The Kinetic energy of the system can be written as:

$$T_{total} = T_M + T_b \tag{6}$$

where:
$T_M$: Kinetic energy of the rotor.
$T_b$: Kinetic energy of the unbalance mass.

hence,

$$T_M = \frac{1}{2}M(\dot{x}^2 + \dot{y}^2) + \frac{1}{2}I_o(\dot{\theta} + \dot{\gamma})^2 \tag{7}$$

and,

$$T_b = \frac{1}{2}m_b {v_b}^2 \tag{8}$$

where:
$v_b$: unbalanced mass velocity.

the position of the unbalance mass at an instant can be written as:

$$\overrightarrow{x_b} = [x + e\cos(\theta + \gamma)]i + [y + e\sin(\theta + \gamma)]j \tag{9}$$

taking the time derivative of $\overrightarrow{x_b}$, this yields

$$\frac{d}{dt}\overrightarrow{x_b} = \overrightarrow{v_b} = \left[\dot{x} - e\left(\dot{\theta}+\dot{\gamma}\right)\sin(\theta+\gamma)\right]i + \left[\dot{y} + e(\dot{\theta} + \dot{\gamma})\cos(\theta+\gamma)\right]j \quad (10)$$

by squaring both sides and simplifying, $v_b^2$ can be found as:

$$v_b^2 = \left\{\dot{x} - e\left(\dot{\theta}+\dot{\gamma}\right)\sin(\theta+\gamma)\right\}^2 + \left\{(\dot{y} + e(\dot{\theta} + \dot{\gamma})\cos(\theta+\gamma)\right\}^2 \quad (11)$$

Substitute in Eqn. 8,

$$T_b = \frac{1}{2}m_b\left[\left\{\dot{x} - e\left(\dot{\theta}+\dot{\gamma}\right)\sin(\theta+\gamma)\right\}^2 + \left\{(\dot{y} + e(\dot{\theta} + \dot{\gamma})\cos(\theta+\gamma)\right\}^2\right] \quad (12)$$

Then the $T_{total}$ can be written as:

$$T_{total} = \frac{1}{2}M(\dot{x}^2+\dot{y}^2) + \frac{1}{2}I_o(\dot{\theta}+\dot{\gamma})^2 + \left(\frac{1}{2}m_b\right)\left[\left\{\dot{x} - e\left(\dot{\theta}+\dot{\gamma}\right)\sin(\theta+\gamma)\right\}^2 + \left\{(\dot{y} + e(\dot{\theta} + \dot{\gamma})\cos(\theta+\gamma)\right\}^2\right] \quad (13)$$

The system's total potential energy can be divided into three terms, namely, $U_x$, $U_y$ and $U_{tor}$. Where $U_x$, $U_y$ and $U_{tor}$ are the potential energies along the *x, y* and torsional direction, respectively. Therefore, the total potential energy can be written as follows:

$$U_{total} = U_x + U_y + U_{tor} \quad (14)$$

where

$$U_x = \frac{1}{2}K_b x^2$$

and,

$$U_y = \frac{1}{2}K_b y^2$$

The bending stiffness ($K_b$) in the above Equations is a function of the material property, geometry and applied boundary conditions.

In this work, the test specimen is assumed to be a beam fixed at both ends (fixed bearing condition) with a concentrated load at its center resulting from the centrifugal force of the eccentric mass. The formula for the maximum deflection taking place at midspan is given by the following:

$$\Delta_{max} = \frac{PL^3}{192\,EI} \quad (15)$$

The bending stiffness is defined as:

$$K_b = \frac{P}{\Delta}$$

Substitute in Eqn. (15) gives the bending stiffness for a fixed bearing conditions:

$$K_b = 192\frac{EI}{L^3} \quad (16)$$

where:
$E$: Material's modulus of elasticity.
$I$: Second moment of area of tested specimen.
$L$: Length of tested specimen.
$P$: Applied load at the center.

Eq. (16) was validated numerically using finite element analysis for a pipe fixed at both ends and rotating around its axis.

The potential torsional energy can be written as

$$U_{tor} = \frac{1}{2}K_{tor}\gamma^2 \quad (16)$$

Similar to the bending stiffness, torsional stiffness ($K_{tor}$) is defined as the applied torque over the resulting angle of twist.

Therefore, torsional stiffness $K_{tor}$ can be written as:

$$K_{tor} = \frac{T}{\gamma}$$

and the angle of twist is

$$\gamma = \frac{TL}{GJ}$$

where:
$G$: Material's modulus of rigidity
$J$: Polar moment of inertia of the tested specimen

Hence, $K_{tor}$ is can be written as

$$K_{tor} = \frac{T}{\frac{TL}{GJ}} = \frac{GJ}{L} \quad (17)$$

The total potential energy yields:

$$U_{total} = U_x + U_y + U_{tor} = \frac{1}{2}K_b x^2 + \frac{1}{2}K_b y^2 + \frac{1}{2}K_{tor}\gamma^2 \quad (18)$$

Now the torsional motion component has been successfully derived. Similarly, the non-conservative energy component can be developed as follows:

$$D_{total} = \frac{1}{2}c_b\dot{x}^2 + \frac{1}{2}c_b\dot{y}^2 + \frac{1}{2}c_{tor}\dot{\gamma}^2 \quad (19)$$

where, $c_b$ and $c_{tor}$ are

$$c_b = 2\zeta_b w_{n,b}(M + m_b)$$

$$c_{tor} = 2\zeta_{tor} w_{n,tor}(I_o + m_b e^2)$$

and other terms ($\zeta_b$ , $\zeta_{tor}$, $w_{n,b}$ and $w_{n,tor}$ ) respectively represent selected bending, torsional damping ratios, bending and torsional natural frequencies. $w_{n,b}$ and $w_{n,tor}$ can be defined as

$$w_{n,b} = \sqrt{\frac{K_b}{M + m_b}}$$

$$w_{n,tor} = \sqrt{\frac{K_{tor}}{I_o + m_b e^2}}$$

Lagrange equation which was given in Eq. (4) can be written as:

$$L = T_{total} - U_{total}$$

$$L = \left[\frac{1}{2}M(\dot{x}^2 + \dot{y}^2) + \frac{1}{2}I_o\left(\dot{\theta} + \dot{\gamma}\right)^2 + \left(\frac{1}{2}m_b\right)\left[\{\dot{x} - e\left(\dot{\theta} + \dot{\gamma}\right)\sin(\theta + \gamma)\}^2 + \{(\dot{y} + e(\dot{\theta} + \dot{\gamma})\cos(\theta + \gamma)\}^2\right]\right] - \left[\frac{1}{2}K_b x^2 + \frac{1}{2}K_b y^2 + \frac{1}{2}K_{tor}\gamma^2\right] \quad (20)$$

Utilizing Lagrange formulation in three degrees of freedom (Eq. 5), yield the following three equations of motion for the system:

$$(M + m_b)\ddot{x} + c_b\dot{x} + k_b x = m_b e\left[\left(\ddot{\theta} + \ddot{\gamma}\right)\sin(\theta + \gamma) + \left(\dot{\theta} + \dot{\gamma}\right)^2\cos(\theta + \gamma)\right] \quad (21)$$

$$(M + m_b)\ddot{y} + c_b y + k_b y = m_b e\left[\left(\dot{\theta} + \dot{\gamma}\right)^2\sin(\theta + \gamma) - \left(\ddot{\theta} + \ddot{\gamma}\right)\cos(\theta + \gamma)\right] \quad (22)$$

$$I\ddot{\gamma} + c_{tor}\dot{\gamma} + k_{tor}\gamma = m_b e[(\ddot{x}\sin(\theta + \gamma)) - (\ddot{y}\cos(\theta + \gamma))] + T_{tor} \quad (23)$$

where, $I = I_o + m_b e^2$

Eqs. (21-23) are nonlinear ordinary differential equations. These set of equations were solved numerically using fourth-order Runge–Kutta Algorithm in Matlab software. The outcome of applying this Algorithm is presented in the results and discussion section. This work considered the single step scheme using the versatile fourth order Runge-Kutta Algorithm instead of the basic Euler solver and other ODE solvers as it is more efficient, accurate and can be implemented with minimal additional work. Taking computational effort and step size into account, the Runge-Kutta Algorithm computes a solution value that is near the limits imposed by machine accuracy (in single precision arithmetic). The goal was to arrive at a decent approximation to the initial value problem. For instance, the authors noticed that an ODE solver such as the Euler Method spirals away from the exact periodic solution, whereas the 4th order Runge-Kutta Algorithm performs rather well.

## EXPERIMENTAL APPROACH

A novel in-house experimental setup capable of imitating downhole lateral and torsional vibrations has been designed and constructed. In this work, vibration coupling effects and interactions between various phenomena such as whirling, and parametric excitation are investigated. Parameters of experimental setup have been adopted to validate the previously developed mathematical model. A major focus of the setup is to experimentally examine the coupling impact on the fatigue life of drill string. This helps reducing drill string failures as well as provides satisfactory answers and justifications about uncertainty and performance of the drill string under various loading and operating conditions. Subsequent sections discuss briefly limitations, constraints, design specifications, design development and construction of the experimental setup.

### Limitations and Constraints

- The length of the setup and drillstring are kept small due to the space limitations and to provide easy mobility. The length of experimental setup is 6.0 m and the length of the drillstring is 5.0 m. The length of the portion of the drillstring between both chucks is 4 m.
- Due to restrictions in dimensions, drillstring diameter and thickness are also reduced in order to initiate a more realistic cycles of fatigue failure.
- Drillstring with diameters of (1.0", 2.0", and 3.0") were used.
- Drillstring thicknesses are varied from one drillstring to another. Drillstring thicknesses of 5mm, 4mm, and 3mm are used.
- The tested drillstrings are allowed to freely rotate and fixed at the top and bottom ends to simulate real-world drilling conditions.
- Since lateral vibrations are recognized as the leading cause of drill string and BHA failures, the experiments were initially designed to account for the effect of lateral vibrations on the fatigue life of the drill string.
- Coupling impact of lateral and torsional vibrations are also examined. The torsional vibration is induced using the setup braking mechanism.
- Further investigations to account for the consequence of applying various torsional loadings are ongoing research.

**Experimental Setup**

The experimental setup (Fig. 3) mainly consists of the following: a testing tube represents the drill string: a support system that includes supporting plates fixed to ground to provide stability for the facility: C-Channels beams to connect the supporting tables; a loading and rotation mechanism which includes motor, sprocket, chain, chucks, pillow bearings, connections, flanges and housing pipes; stabilizers representing the wellbore; a control unit and speed invertor; a sensing mechanism that includes torque measurement system for measuring top and bottom torques, Hall Effect for measuring rotational speed, number of cycles, and ultrasound sensors for measuring vibration amplitude; a braking mechanism is utilized to induce reversed torque at the other end of the drill string; and a data acquisition system that includes a twelve channels data logger and computer. Fig. 3a shows an image of the experimental setup while Fig. 3b shows a schematic of the setup and its individual components. Fig. 3c shows torque measurement system fixed to the drill string. The representations for the numbers indicated on Fig. 3b are listed in Table 1.

(a)

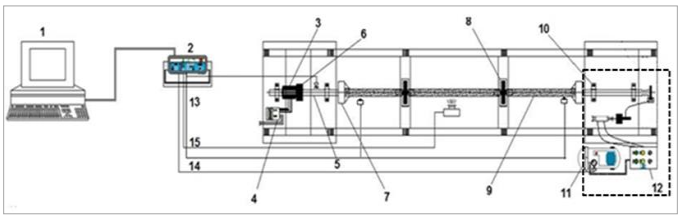


(b)

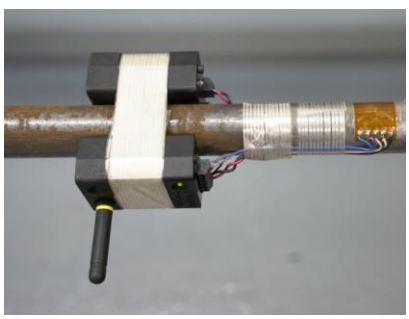

(c)

**Fig. 3.** Experimental Setup (a: image of experimental setup and loading mechanism, b: schematics shows individual components, c: torque measurement system)

**Table 1**: Main components of the experimental setup

| COMPONENTS/ SYSTEMS | PART NAME |
|---|---|
| 1 | Computer |
| 2 | Data acquisition system |
| 3 | 3-plase electrical motor |
| 4 | Speed controller |
| 5 | Shaft |
| 6 | Sprocket and Chain |
| 7 | Chuck and flange assembly |
| 8 | Stabilizer |
| 9 | Specimen (Tube) |
| 10 | Ball bearing |
| 11 | Compressor |
| 12 | Brake system controller |
| 13 | Hall effect sensor |
| 14 | Brake on/off switch |
| 15 | Ultrasonic sensor |
| 16 | Torque Measurement System |

The setup structural support consists of two 16 mm thickness mild steel tables, ring shape stabilizers and four C-channel connecting the tables to the stabilizers and providing stability to the setup. The C-channels are fixed to a concrete floor. The structural provides safe working environment and holds other mechanism such as the rotation mechanism and braking system. The chuck is connected to the housing pipe as shown in Fig. 3a. The same mechanism is fixed on the other side of the setup. The housing pipes allow the drill string guided through it for about 0.5 m on each side to give stability and rigidity for the drill string. The housing pipes are also guided through two ball bearings, to give support and allow smooth rotation. The total length of the specimen is 6 m whereas the length between the two chucks is 5 m since a total of 1 m of the specimen is guided inside the housing pipes.

**Testing Procedure**

Numbers of mild steel tubes represent drill strings of various outer diameters (1", 2", and 3") used in this work. The drill string is rotated through 12-hp motor using (sprocket/chain) power transmission component. A speed inverter (Variable Frequency Drive) is utilized to regulate the angular speed of the drill string. Lateral vibration is induced in the drill string by adding eccentric mass as shown in Fig 4. To induce torsional vibration, a braking mechanism is adopted. In this work, the breaking mechanism is constrained to brake at fixed duration and steady applied torque while allowing multiple numbers of brakes. Variation of applied torque and intervals will be considered in our ongoing research study. Braking produces a reverse torque on the drill string with

the risk of unscrewing of the drill string, and hence introduces a twisting angle. In this work, the angular speed, lateral amplitude, and the applied and reverse torque are measured using speed inverter, Hall Effect, and torque measurement system, respectively. High performance universal data loggers (as shown in Fig. 5) with 24-bit analogue-to-digital converters and up to 16 universal channels have been used to process and display results.

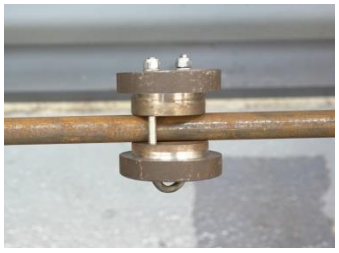

**Fig. 4.** Unbalanced mass ($m_b$)


**Fig. 5.** Standalone date logger

## RESULTS AND DISCUSSION

### Methods of resolution of mathematical model

In this work a mathematical model of a drilling pipe was successfully presented. The system's equations of motion were derived using Lagrange's Equations as introduced in above section. These equations were solved numerically by using a Runge Kutta algorithm in Matlab software. The model was first examined using readily measured parameters and other calculated parameters as listed in Table 1.

Table 1: Experimental and calculated parameters

| PARAMETER | VALUE | UNIT |
|---|---|---|
| $c_b$ | 0.2 | $N.s/m$ |
| $c_{tor}$ | $3e^{-4}$ | $N.m.s/rad$ |
| $e$ | 0.05 | $m$ |
| $M$ | 9 | $kg$ |
| $m_b$ | 2.5 | $kg$ |
| $K_b$ | 1 | $N/m$ |
| $K_{tor}$ | 0.05 | $N.m/rad$ |

### Undamped rotor rotating at critical speed:

The undamped system is examined and shown that the critical speed occurs when $\dot{\theta} = w_{n,b}$. and $c_b = 0$ . Fig. 6 shows that lateral deflections are continuously increased as undamped system is operated at its critical speed. Hence, rotating close to its critical speed maximum values of deflections are reached. Operating at a speed greater or lower than the critical speed would result in a smaller deflection values. Therefore, the subsequent investigations are carried at the rotor's critical speed as it represents the worst case scenario. Fig. 7 shows trajectories of horizontal and vertical deflections of undamped shaft rotating at critical speed.

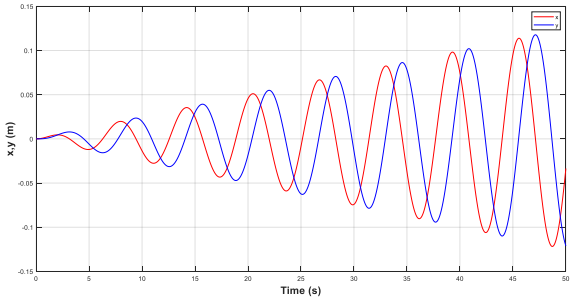


**Fig. 6**. Undamped system lateral deflections

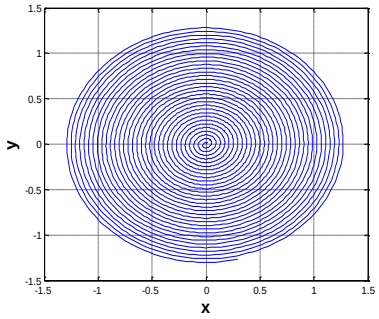


**Fig. 7.** Trajectories horizontal and vertical deflections of undamped shaft

### Effect of Bending damping ratio on rotor's response

The effect of bending damping ratio on the rotor's response was investigated by changing the value of the damping coefficient. The effects of changing damping ratio ($\zeta_b = 0.05, 0.07$ & $0.1$) on transient response and magnitude of deflection were observed. It can be depicted in Figure 8.a, 9.a and 10.a and their trajectories in Figure 8.b, 9.b and 10.b that by increasing the bending ratio, the time required to reach steady state response and deflections are reduced. This is due to the increase in the dissipated energy of the system. For instance, in Fig. 8a steady state response was reached at 1.3 seconds. However, it is around 1.2 and 1.0 as shown in Figs. (9.a & 10.a).

1. Bending damping ratio $\zeta_b = 0.05$

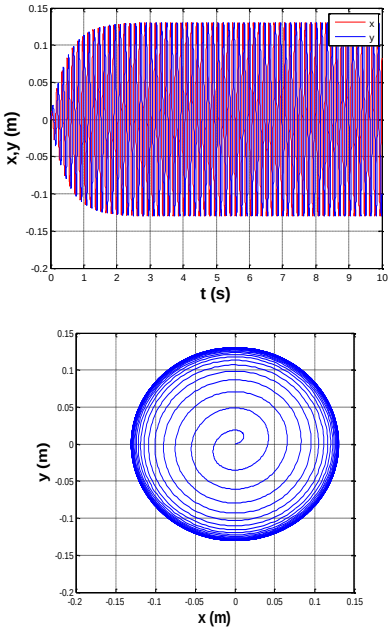


**Fig. 8 a and b** Effects of changing damping ratio at $\zeta_b = 0.05$

2. Bending damping ratio $\zeta_b = 0.07$

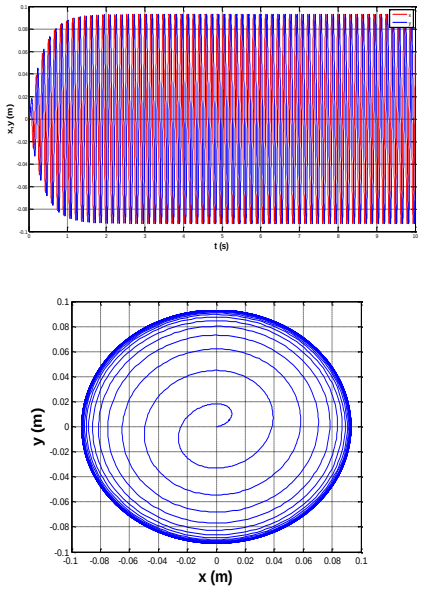


**Fig. 9a and b** Effects of changing damping ratio at $\zeta_b = 0.07$

3. Bending damping ratio $\zeta_b = 0.1$

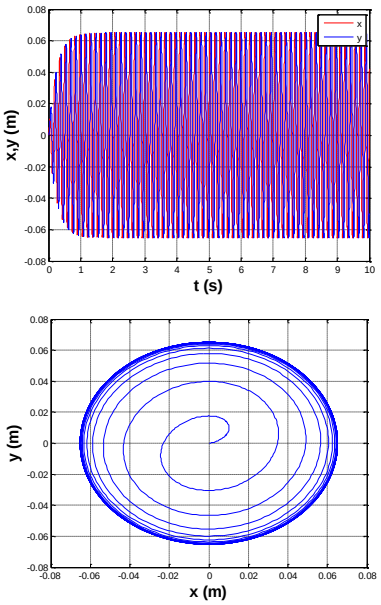


**Fig. 10 a and b** Effects of changing damping ratio at $\zeta_b = 0.1$

**Effect of unbalanced mass on rotor's response**

The effect of unbalanced mass on the rotor's response is investigated. It can be noticed from Figs. 11 (a and b), 12 (a and b) and 13 (a and b) that when the unbalanced mass (1kg, 3kg and 5kg) is increased, the lateral deflection is also increased as a consequence of the increase in the centrifugal force while bending damping ratio is kept constant at ($\zeta_b = 0.07$). A steady state is reached at ± 0.035m for unbalanced mass of 1kg. Whereas, the steady state is at 0.09m for 3kg and about 0.13m for 5kg unbalanced mass, respectively.

1. unbalanced mass $m_b = 1kg$ and $\zeta_b = 0.07$

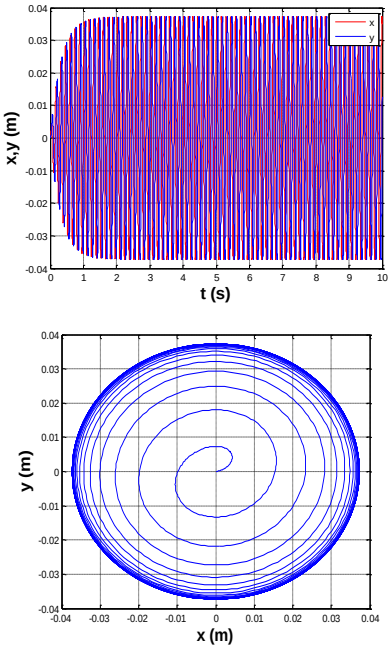

**Fig. 11.** Effect of unbalanced mass on the rotor's response at $m_b = 1kg$ and $\zeta_b = 0.07$

2. Unbalanced mass $m_b = 3kg$ and $\zeta_b = 0.07$

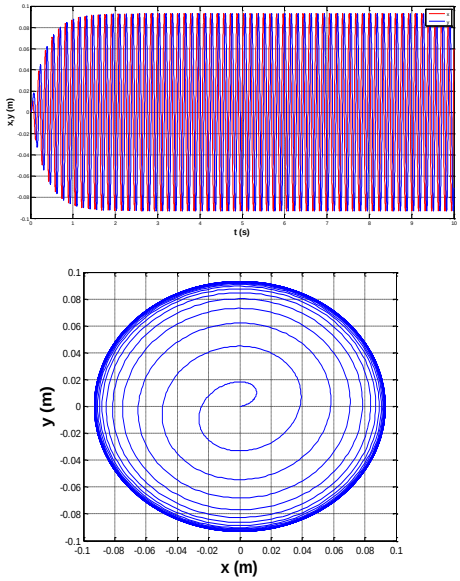


**Fig. 12.** Effect of unbalanced mass on the rotor's response at $m_b = 3kg$ and $\zeta_b = 0.07$

3. Unbalanced mass $m_b = 5kg$ and $\zeta_b = 0.07$

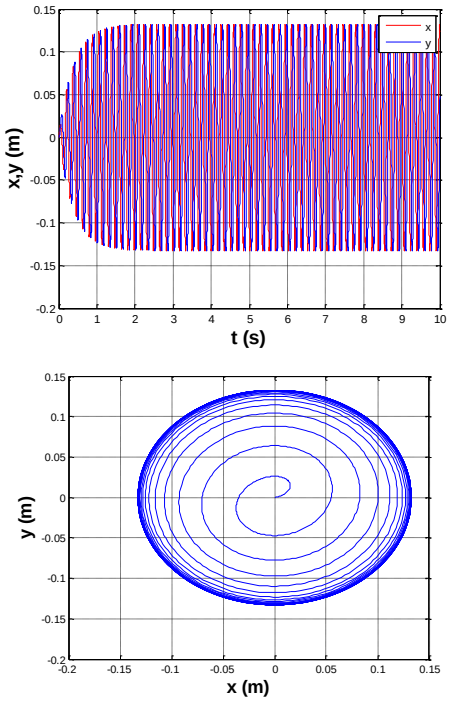


**Fig. 13.** Effect of unbalanced mass on the rotor's response at $m_b = 5kg$ and $\zeta_b = 0.07$

**Effect of applied reverse torque on rotor's response**:
The effect of reverse torque on the rotor's response is also investigated. Figure 14 shows that as the external reversed applied torque is increased, the resulting angle of twist $\gamma$ is increased as well. Figure 15 shows the effect of torque versus normalized total angular speed of the rotor $\dot{\beta}_{norm}$. The results in Figs 14 and 15 are generated for an applied torque equal 70 N.m, 140 N.m, and 180 N.m at the time interval [10-12]. It is noticed that at instants when applied torque is released, a large fluctuation takes place and causes the rotor to momentarily stop and start rotating in the reverse direction with respect to the applied angular speed $\dot{\theta}$. The torsional spring action of the system stores energy and once released it causes the rotor to spin with an angular velocity at least two times greater than $\dot{\theta}$. For instance, at 70 N.m applied reversed torque, the angle of twist ($\gamma$) has changed form - 6° to 1.5°. Similar observations are also noticed in Fig 15.

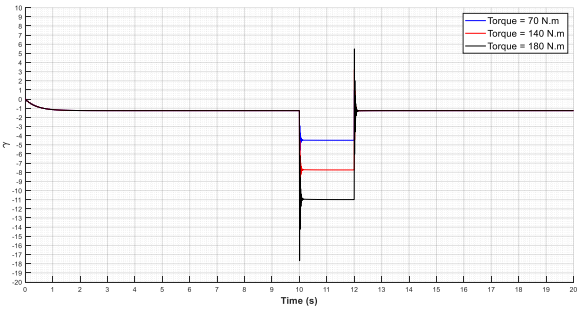


**Fig. 14.** Effect of applied reverse torque on rotor's response at time interval [10-12]

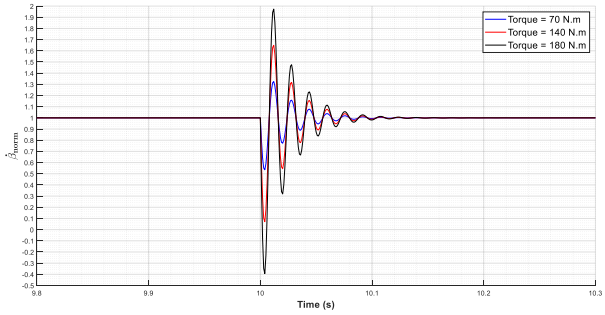


**Fig. 15.** Effect of applied reverse torque on rotor's response at time interval [10-12]

## Experimental results

The experiments were carried out under controlled conditions to examine the setup performance, and to investigate the effects of induced lateral vibration on the drill string fatigue failure. Sets of drill strings of 1", 2" and 3" outer diameter and 5m long were used. Initial tests were performed by rotating the drill string on various rotational speed and lateral amplitudes were observed. Similar tests were carried out for the 2" and 3" drill strings. Fig. 17 shows the rotational speed vs. lateral deflections for the three

drillstrings. Fig. 17 shows that the amplitudes are lower in larger drillstring diameters at same rotational speed. In addition, the lateral amplitude is higher for higher speed for the same drillstring dimensions.

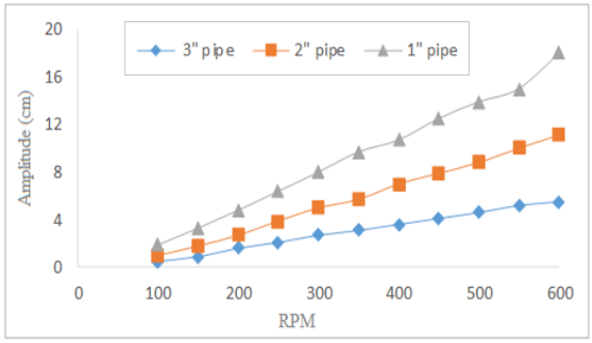


**Fig. 17.** Drill strings behavior at various rotational speeds

Fig. 17 also shows that the lateral amplitude is increased almost linearly when the rotation speed increased. For instance, when the 1" drillstring rotation speed was near its critical speeds the lateral amplitudes were significantly increased as shown in Fig. 17 hinting that any further increase in the rotation speed might lead to yielding of the drillstring. Fig. 18 also illustrates that the maximum lateral amplitude occurs in the middle of the drillstring.

Lateral vibration in a drillstring often results from eccentricity which leads to centripetal forces at particular rotational speeds. This phenomenon is known as "whirl". In real-world applications, the initial eccentricity of the drillstring is due to gravity or weight on bit (high compressive loads) as well as the presence of imbalance lumped mass which is attached to the drillstring as shown in Fig. 18. When external excitations (rotating the drillstring) take place close to lateral natural frequencies, the amplitude of lateral vibration remarkably increases and hence the drillstring strikes wellbore wall and creates considerable shocks.

**Fig. 18.** Large lateral amplitude for 1" drill string near its rotational critical speed.

**Comparison between numerical and experimental results**

Comparison between the numerical results from the established model and the experimental results is performed by introducing the frequency ratio ($\eta$) such as

$$\eta = \frac{\dot{\beta}}{w_b}$$

This has allowed plotting numerical maximum deflection of various pipe's diameters with respect to the frequency ratio as shown in Fig. 19. It can be observed that the maximum deflection continuously increases with respect to the frequency ratio and reaches its critical value at $\eta = 1$ "i.e. $\dot{\beta} = w_b$" which indicates that the total angular speed of the rotor = bending natural frequency of the system. Once the frequency ratio increased beyond the bending natural frequency of the system, the maximum deflections start to decrease. It can be noticed that the maximum deflections are function of the geometrical parameters of the test specimen as deflections decreases significantly for pipes with larger diameters and thickness. The maximum deflections for three pipes rotating at $\eta = 0.9$ (corresponds to 90% of the pipe's critical speed) are measured and compared to the calculated results from the numerical model. The results are presented in Table 3. The results in Fig. 19 and table 3 shows that the numerical model is able to accurately reproduce the experimental results.

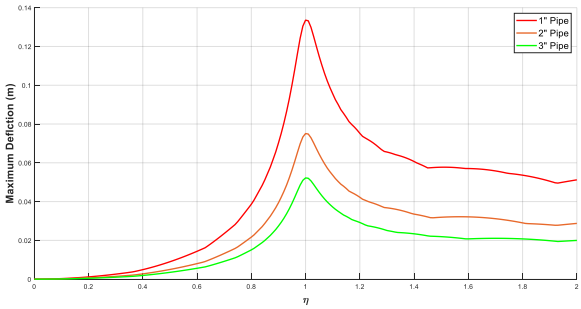


**Fig. 19.** Numerical maximum deflection with respect to the frequency ratio.

Table 3: Comparison between numerical and experimental deflections.

| Drillstring size (outer diameter) | Drillstring inner diameter (mm) | Eccentric mass (kg) | Maximum deflection (numerical) at η =0.9. Fig. 19. | Maximum deflection (experiment) at η =0.9. Measured | Percent error |
|---|---|---|---|---|---|
| 3" (76.2mm) | 68.2 | 2.5 | 73 mm | 77 mm | 5.1% |
| 2" (50.8mm) | 44.8 | 2.5 | 39 mm | 41 mm | 4.9% |
| 1" (25.4mm) | 21.4 | 2.5 | 28 mm | 29 mm | 3.5% |

**Critical speed and critical frequency calculations**

The theoretical critical speed for the 3", 2" and 1" drillstring are calculated and presented in Table 4. Equation (16) is modified and used to calculate the critical frequency and critical speed as follows:

$$w_b(\text{Hz}) = \sqrt{\frac{K_b}{m}} = \sqrt{\frac{192\ EI}{mL^3}}$$

Critical speed (rpm) = $w_b$ x 60

**Table 4**: Theoretical critical frequency and critical rotational speeds of the drillstrings

| Drillstring size | 3" | 2" | 1" |
|---|---|---|---|
| Critical frequency (Hz) | 25.3 | 18.15 | 11.0 |
| Critical speed (rpm) | 1518 | 1089 | 660 |

As an example, the critical frequency and critical speed for the 3" pipe shown in table 4 is calculated using the following parameters: do= 76.2 mm, di= 66.22, t = 5mm, E= 200,000 N/mm2, L= 4000 mm, m = 10.67 Kg, $I = \frac{\pi}{4}(d_o^4 - d_i^4)$.

**Fatigue failure characterization**

The second set of tests was performed to investigate the fatigue failure due to inducing lateral vibration in the drill strings. Drill strings of three sizes (1", 2" and 3") were rotated at various rotational speeds and numbers of cycles to fatigue failure were observed (propagation of cracks corresponding to stage 3). For each diameter of the drill strings a number of samples was utilized. Fig. 20 shows the number of cycles to fatigue failure of different sizes of drillstrings at various rotational speeds. As shown in Fig. 20, number of cycles to failure has decreased as the rotational speed has increased which indicates that rotation speed and drill string sizes are the most significant factors in determining the number of cycles to fatigue failure. Fig. 18 also shows that with a rotational speed of about 10% less than the critical rotational speed (for all drill strings), the numbers of cycles to failure is significantly reduced. This is due to the high lateral amplitude that is induced in each drillstring as the rotation speed of increased to about 90% of the drill string critical rotation speeds. Fig. 21 shows a yielded 1" drillstring after it has been rotated for a few hundreds of cycles. A test was conducted at 94% of the drill string critical speed (620 rpm) and resulted in a deflection (lateral amplitude) of about 11.5 cm. This process would lead to a better understanding of drillstring behavior under such loading condition and hence increase safety measures and reduce uncertainty for oil and gas drilling industry.

For a deeper understanding of the impact of lateral amplitude on the fatigue life of a drill string, an experiment was conducted using a 2" drill string and rotated until constant lateral amplitude was reached and the number of cycles to failure was counted. Utilizing the same diameter of drill string, a similar experiment was performed at higher rotational speed and lateral amplitude and the number of cycles to failure were observed. The tests were repeated at higher rotation speeds and lateral amplitudes. Results presented in Fig. 22 show that the number of cycles to fatigue is increased as the lateral amplitude is reduced. It can be seen from Fig. 22 that when lateral amplitude plotted versus number of stress cycles, the behavior is similar to the familiar fatigue S-N curve for mild steel. In this case, the lateral amplitude represents the fatigue strength versus number of cycles to fatigue failure.

Fig. 23 shows fatigue failure of 1" drill string at around 553110 cycles due to rotating it at 600 rpm (10% lower than the pipe critical speed 660 rpm) and attached eccentric mass of 0.9kg. As it can be seen from Fig. 23 is about 8 cm away from the unbalanced mass.

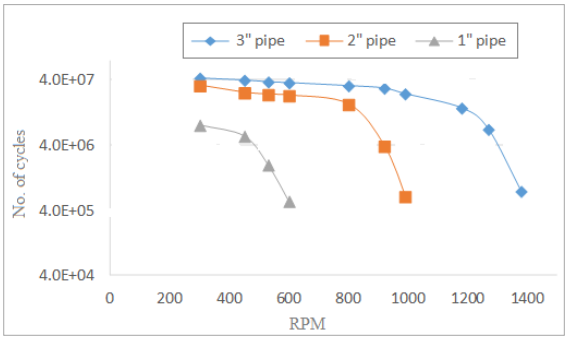


**Fig. 20.** Drillstrings rotational speeds versus number of cycles to fatigue failure.

**Fig. 21.** Yielding of 1" drillstring due to operating at 94% critical speed

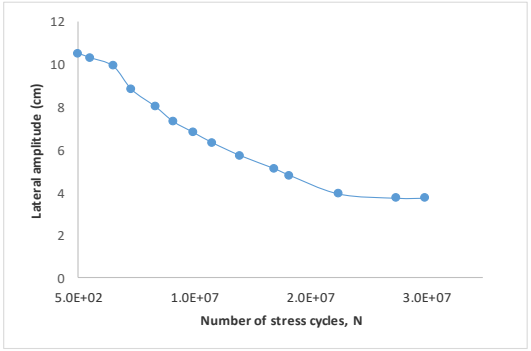


**Fig. 22.** Lateral amplitude Vs number of stress cycles of 2" drillstring

**Fig. 23.** Fatigue failure of 1" drill string

In another experiment and as it was explained in the testing procedure, the torsional vibration is induced in the drill string by applying a constant reversed torque utilizing the braking mechanism in the drill string at multiple number of brakes for a fixed duration (i.e. 5 sec.). Fig. 24 shows number of cycles versus number of braking per minute to fatigue failure at various rotational speeds for 2" diameter drill string. The figure illustrates that when number of braking was higher (i.e., 3 brakes per minute), number of cycles to fatigue failure less for all rotational speeds. However, when number of braking was low (i.e. 1 braking per min), number of cycles to fatigue failure was at highest for all rotational speeds. This indicate that frequent stick-slip occurrence leads to earlier fatigue failure of drill string unless the system's critical operating speeds and design parameters are determined and implemented for a safe drilling.

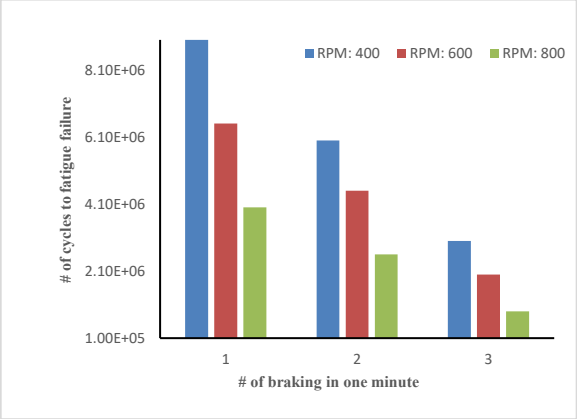


**Fig. 24.** No. of cycles to fatigue failure at constant torque and duration for multiple braking at various RPM

## Conclusions

This work aimed at gaining a deeper understanding of the complex behavior of drill string under vibrations and its detrimental effect on drilling operation. The developed model imitates real drillstring behavior inside the wellbore with regards to its dynamic movements based on modeling an in-house constructed testing rig which mimic the real drilling field operations. Lagrangian approach is used to obtain the drillstring lateral and torsional vibration coupling equations of motion. A mathematical model is developed to simulate the dynamic behavior of the drillstring. The effects of lateral and torsional vibrations and whirling motion of the drillstring are included in the model. An experimental setup was developed to imitate the vibration modes induced in the drillstring when it runs downhole in oil or gas wells. The testing facility is capable of investigating effects of individual and coupled modes on vibration on drill string failure. The performance of the setup was validated. A relationship between the rotation speed and drillstring vibration lateral and torsional amplitudes were established for various drillstring sizes. Fatigue failure tests were performed and showed that the drill string size, rotation speed, laterals and torsional vibration amplitudes have significant effects on fatigue life of the drillstring. Results showed that operating on a rotation speed higher than 90% of the drillstring critical speed leads to yielding of the drill string. Results also showed that the lateral amplitude versus number of stress cycles behavior is similar to the familiar fatigue S-N curve. Torsional vibration is induced in the drill string by applying a constant reversed torque utilizing the braking mechanism in the drill string at multiple numbers of brakes. Results showed that multiple numbers of braking, which represent frequent stick-slip, leads to fatigue failure unless the system's critical operating speeds and design parameters are determined and implemented for a safe drilling. The developed model predicted that the vibrations induced in the drill string due to the interaction with the wellbore are the main reason for drill string failure. Unlike previous work, this model established a method for determining the critical operating speeds and design parameters for a safe drilling. It also provided a basis for developing a fatigue failure model that can predict the safe operating life of drill string.

## ACKNOWLEDGMENT

This publication was made possible by NPRP grant # [8-690-2-298] from the Qatar National Research Fund (a member of Qatar Foundation). The findings achieved herein are solely the responsibility of the authors.

## REFERENCES

[1] Macdonald, K.A., Bjune, J.V., 2007, "Failure analysis of drillstrings," Engineering Failure Analysis, 14, pp. 1641-1666.
[2] Moradi, S., Ranjbar, K., 2009, "Experimental and computational failure analysis of drillstrings. Engineering Failure Analysis," 16, pp. 923-933.
[3] Reid, D., Rabja, H., 1995, "Analysis of drill string failure," Presented in 1995 SPE drilling conference, Amsterdam.

[4] Jardine, S., Malone, D., Sheppard, M., 1994, “Putting a damper on drilling’s bad vibrations,” Oilfield Review, 1, pp. 15-20.
[5] Spanos, P.D., Chevallier, A.M., Politis, N.P., Payne, M.L., 2003, “Oil well drilling: a vibrations perspective,” The Shock and Vibration Digest, 35(2), pp. 81-99.
[6] Khulief, Y.A., Al-Naser, H., 2005, “Finite element dynamic analysis of drill strings,” Finite Element Analysis and Design, 41, pp. 1270-1288.
[7] Berlioz, A., Der Hagopian, J., Dufour, R, Draoui, E., 1996, “ Dynamic behaviour of drill-string: experimental investigation of lateral instabilities,” Transaction of the American Society of Mechanical Engineers, Journal of Vibration and Acoustics, 118(3), pp. 292-298.
[8] Yigit, A.S., Christofourou, A.P., 1996, “Coupled axial and transverse vibrations of oil well drillstrings,” Journal of Sound and Vibration, 195(4), pp. 617-627.
[9] Baryshnikoy, A., Calderoni, A., Ligrone, A., Ferrara, P., 1997, “A new to the analysis of drillstring fatigue behaviour,” SPE Drilling and Completion, 12(2), pp. 77-84.
[10] Abdo, J., 2011, “Analytical approach to estimate amplitude of stick-slip oscillations,” Journal of Theoretical and Applied Mechanics, 49(4), pp 971-986.
[11] Farhang, K., Lim, A., 2007, “A kinetic friction model for viscoelastic contact of nominally flat rough surfaces,” Journal of Tribology, 129 (3), pp. 684-688.
[12] Yigit, A.S., Christoforou, A.P., 1998. Coupled torsional and bending vibrations of drillstrings subject to impact with friction. Journal of Sound and Vibration. 215(1), 167–181.
[13] Ghasemloonia, A., Rideout, D.G., Butt, S.D., 2015. A review of drillstring vibration modeling and suppression methods. Journal of Petroleum Science and Engineering. 131(1), 150-164.
[14] Abdo, J., 2006, “Modelling of Frictional Contact Parameters of a Mechanical Systems,” International Journal of Applied Mechanics and Engineering, 11(3), pp 449-465.
[15] J. Abdo, E. Hassan, A. Al-Shabibi and J. Kwak (2017) “Design of a Testing Facility for Investigation of Drill Pipes Fatigue Failure” The Journal of Engineering Research V. 14 (2), p 1-7.
[16] Ahmadian, H., Nazari, S., Jalali, H., 2007, “Drill string vibration modelling including coupling effects,” IUST International Journal of Engineering Science, 18(3-4), pp. 59-66.
[17] Finnie, I., Bailey, J.J., 1960, “An experimental study of drill string vibration,” American Society of Mechanical Engineers, Journal of Engineering for Industry, 82(2), pp. 129-135.
[18] Yigit, A.S., Christoforou, A.P., 1998, “Coupled torsional and bending vibrations of drill string s subject to impact with friction,” Journal of Sound and Vibration, 215, pp 167-181.
[19] Vandiver, J.K., Nichoison, J.W., Rong-Juin, S., 1991, “Case studies of the bending vibration and whirling motion of drill collars,” SPE, Drilling Engineering, pp. 282-290.
[20] Jansen, J.D., 1991, “Non-linear rotor dynamic as applied to oil well drill string vibrations,” Journal of Sound and Vibration, 147, pp. 115-135.
[21] Jansen, J.D., Steen, L., Zachariasen, E., 1995, “Active damping of torsional drill string vibrations with a hydraulic top drive,” SPE Drilling & Completion, 10(4), pp. 250-254.
[22] Dunayevsky, V.A., Abbassian, F., 1998, “Application of stability approach to torsional and lateral bit dynamic,” SPE Drilling & Completion, 13(2), pp 99-107.
[23] Nouby, M., Abdo J., Mathivanan D., Srinivasan K., “Evaluation of disc brake materials for squeal reduction,” Tribology Transactions, 2011.
[24] Yigit, A.S., Christoforou, A.P., 2000. Coupled torsional and bending vibrations of actively controlled drillstrings. Journal of Sound and Vibration. 234(1), 67–83.
[25] Elsayed, M.A., Raymond, D.W., 2002. Analysis of coupling between axial and torsional vibration in a compliant model of a drillstring equipped with a PDC bit. In: Proceedings of the ASME 2002 Engineering Technology Conference on Energy (ETCE). Houston, Texas.
[26] Abdo, J., 2006 “Investigation of contact stiffness and its relation to friction induced noise and vibration,” International Journal of Modelling and Simulation, 26(4), pp 295-302.
[27] Zamanian, M., S.E. Khadem, S.E., Ghazavi, M.R., Stick-slip oscillations of drag bits by considering damping of drilling mud and active damping system, Journal of Petroleum Science Engineering 59 (3) (2007) 289–299.
[28] Kapitaniak M, Vaziri V, Páez Chávez J, Wiercigroch M. Numerical Study of Forward and Backward Whirling of Drill-String. ASME. J. Comput. Nonlinear Dynam. 2017;12(6).
[29] Jeffcott H., The lateral vibrations of loaded shafts in the neighbourhood of a whirling speed – the effect of want of balance Philos Mag, 37 (1919), pp. 304-314.
[30] Abdo J., Shamswldin E, Experimental Technique for characterization of friction in dry contact, 2007. Jornal of solid mechanics and materials engineering, 1(10), 1197-1208.
[31] Melakhessou, H., Berlioz, A., Ferraris, G., 2003. A nonlinear well-drill-string interaction model. J. Vib. Acoust. 125 (1), 46-52.
[32] Huang,D.G, 2007, Characteristics of torsional vibrations of a shaft with unbalance, Journal of Sound and Vibration, 308 (3-5), pp. 692-698
[33] Vlajic, N., Liu, X., Karki, H., & Balachandran, B. (2014). Torsional oscillations of a rotor with continuous stator contact. International Journal Of Mechanical Sciences, 8365-75. doi:10.1016/j.ijmecsci.2014.03.025
[34] Vlajic, N., Champneys, A.R., Balachandran, B., (2017) “Nonlinear dynamics of a Jeffcott rotor with torsional deformations and rotor-stator contact”, International Journal of Non-Linear Mechanics 92, 102–110.